Journal of Ovonic Research Vol. 11, No. 5, September - October 2015, p. 195 - 201

EFFECT OF GRINDING TIME ON THE STRUCTURAL AND MAGNETIC PROPERTIES OF ULTRAFINE $Ni_{0.7}Zn_{0.3}Fe_2O_4$

A.A. AZAB[a*], S. ALBAAJ[b]
[a]*Solid State Electronics Laboratory, Solid State Physics Department, Physics Division, National Research Centre, Dokki, Giza, P.O. 12622, Egypt*
[b]*Physics Department, Faculty of Science, Damascus University, Syrian Arab Republic*

Nanocrystalline $Ni_{0.7}Zn_{0.3}Fe_2O_4$ was prepared by solid-state reaction from stoichiometric mixture of ZnO, NiO, Fe_2O_3 powders. After preparation, it was grinded at different times. The X-ray powder diffractometry (XRD), transmission electron microscopy (TEM), Fourier transform infrared spectroscopy (FTIR) and vibrating sample magnetometer (VSM) were carried out to investigate the structural and magnetic properties of $Ni_{0.7}Zn_{0.3}Fe_2O_4$ compounds. The results showed that the compound has nano- structure in which the crystallite size decreases with increasing grinding time. The hysteresis loops at room temperature suggest superparamagnetic like behavior of the nanoparticles. The saturation magnetization decreases with increasing grinding time. The coercivity (Hc) increases with grinding time to a maximum value at grinding time of 30 min and then decreases due to transition from multi domain to single domain state.

(Received May 5, 2015; Accepted September 17, 2015)

Keywords: Ni–Zn ferrite, IR, TEM, Magnetic properties, superparamagnetism

1. Introduction

Nanostructure mixed spinel ferrites have various applications in many areas of science and technology such as magnetic transformer cores, magnetic recording, spintronic devices, ferrofluids, targeted drug delivery, bio-sensors, and telecommunication [1–6]. The properties of ferrites are highly sensitive to the preparation methodology, sintering conditions and impurity levels present in or added to them. For various applications of ferrites, the most important properties are saturation magnetization, Curie temperature, permeability, resistivity and dielectric losses. These properties can be controlled by varying the preparation technique, by introducing additives or by varying the composition. Among Ni–Zn ferrite is of special interest because it can be considered as a mixed ferrite of Ni- and Zn-ferrites. It is well known that $NiFe_2O_4$ has inverse spinel structure, whereas $ZnFe_2O_4$ has normal spinel one [7]. $NiFe_2O_4$ is a ferrimagnetic while $ZnFe_2O_4$ is paramagnetic [7]. Ni–Zn ferrites are soft ferrimagnetic materials having low magnetic coercivity and high resistivity values [8] and little eddy current loss in high frequency operations (10–500 MHz) [9]. Its high electrical resistivity and good magnetic properties make this ferrite an excellent core material for power transformers in electronics, recording heads, and antenna rods, loading coils, microwave devices and telecommunication applications [10–12]. In this work the effect of grinding time on nanocrystalline $Ni_{0.7}Zn_{0.3}Fe_2O_4$ ferrite synthesized by standard ceramic technique from oxide powders is investigated. The structure and magnetic properties of prepared material are presented and discussed along with the formation mechanism and structural evolution during different times of grinding.

*Corresponding author: aliazab@hotmail.com

2. Experimental techniques

$Ni_{0.7}Zn_{0.3}Fe_2O_4$ spinel ferrite was prepared using the standard ceramic technique. Pure oxides (NiO, ZnO and Fe_2O_3) of 99.9% purity were used. The powders were mixed in stoichiometric proportion and grinded in electric coffee grinder for different times 10, 20, 30, and 40 min. The powder was then sintered at 800 ^oC for 8 hrs. The sintered powder was again grinded for 5 min and palletized. The pellets were sintered at 1100 ^oC for 8 hrs and then cooled to room temperature through 24 hrs. Finally the powders were grinded for different times 10, 20, 30 and 40 min. The crystal structure of the powders was investigated by Proker D-8 X-ray diffractometer model PW3710 utilizing Cuk_α radiation (λ= 1.5418 Å) in the 2θ range of 20–80^o. The morphology of the particle was analyzed using transmission electron microscopy (JEOL 2010). Infrared spectroscopic analysis was carried out using Jasco 300E Fourier transform infrared spectrometer. Magnetic properties were studied using a Lake Shore vibrating sample magnetometer (VSM) model 7410 with a maximum applied magnetic field 15 kOe.

3. Results and discussion

3.1. XRD analysis

The XRD patterns of $Ni_{0.7}Zn_{0.3}Fe_2O_4$ grinded at different times 0, 10, 20, 30 and 40 min are shown in Fig. 1. All peaks could be indexed to a single spinel structure according to standard data card no. 89-4927 without any secondary phases. The crystallite size is calculated from the most intense peak of X-ray spectrum using the Debye-Scherrer's equation $D=0.9\ \lambda/\beta\cos\theta$ where β is the corrected full width at half maximum intensity of the peak, λ is the target wavelength and θ is the degree corresponding to the peak position. The crystallite size is ranging from 41.63 nm at zero time grinding and 28.07 nm at time 40 min. It can be noted from table 1, that the crystallite size decrease with increasing time of grinding as expected and as reported by others [13-15]. The lattice parameter is calculated from the equation $a = d\sqrt{h^2 + k^2 + l^2}$. The relation between grinding time and lattice parameter is shown in table 1. The lattice parameter deceases slowly with increasing the time of grinding; which can be due to decreasing in crystallite size. The X-ray density is calculated from the equation $Dx=8M/Na^3$ where M is the molecular weight, N is Avogadro's number and a is the lattice constant. The X-ray density calculated and reported in table 1, its values increases slowly with increasing grinding time, this behavior is in well agreement with the change in lattice parameter.

Table 1. Lattice parameter (a), crystallite size, X-ray density (Dx) and absorption bands frequency (ν_1, ν_2 and ν_3) for $Ni_{0.7}Zn_{0.3}Fe_2O_4$ as prepared and grinded at different times.

X	a (Å)	Cry. size	Dx (g/cm3)	ν_1	ν_1\	ν_2
0	8.417	41.63	5.26	564.07	786.81	442.58
10 min.	8.417	36.73	5.26	562.14	781.02	440.65
20 min.	8.416	33.32	5.27	551.54	778.13	434.86
30 min	8.409	31.18	5.28	546.74	774.27	432.94
40 min	8.414	28.07	5.27	556.37	780.03	434.85

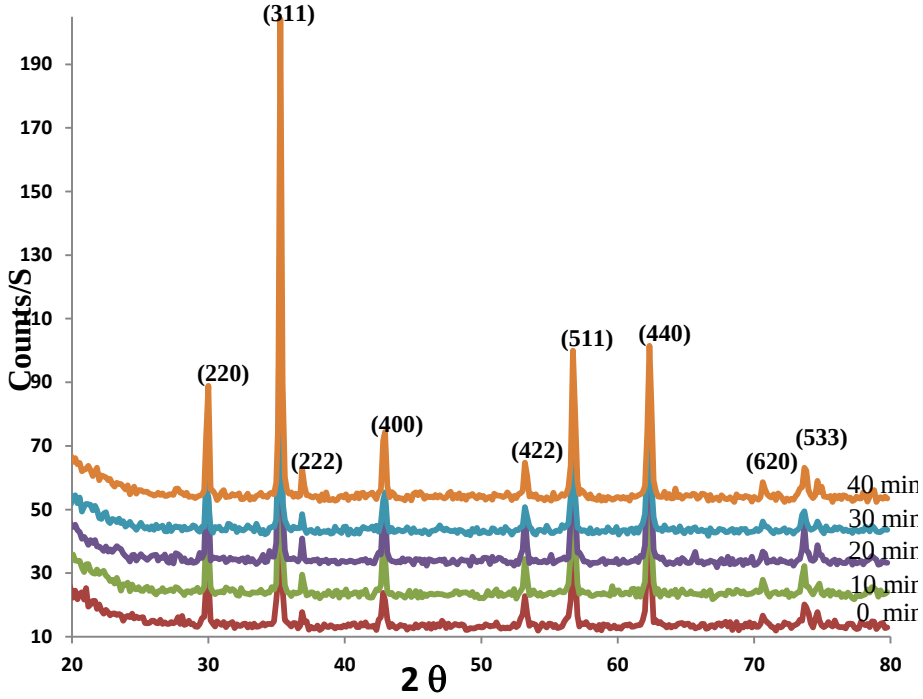

Fig. 1 X-ray diffraction patterns of $Ni_{0.7}Zn_{0.3}Fe_2O_4$ grinded at different times.

3.2. Morphology

Fig. 2 shows the TEM images of $Ni_{0.7}$ $Zn_{0.3}Fe_2O_4$ grinded at 10 and 40 min. The images reveal that particles are in nanometer range, nearly spherical in shape and agglomerated. The particles are nearly homogeneously distributed, being in the size range of 32 nm and 28 nm for samples grinded for 10 and 40 min respectively. The particle size decreases with increasing of grinding time, which supports X-ray results.

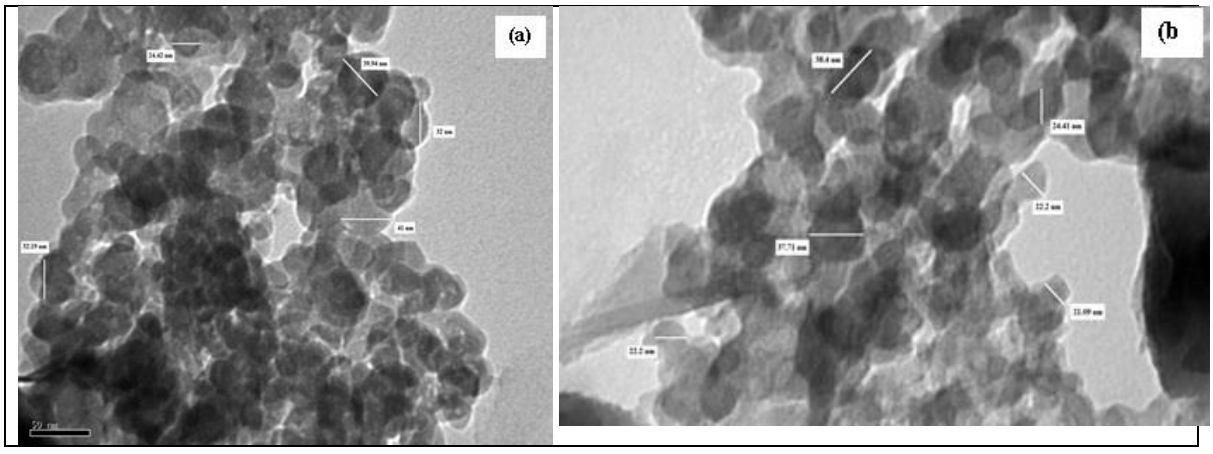

Fig. 2 TEM micrograph of $Ni_{0.7}Zn_{0.3}Fe_2O_4$ grinded at (a) 10 min. (b) 40 min.

3.3 Infrared (IR) spectra

Fig 3 shows the typical FTIR spectra of $Ni_{0.7}$ $Zn_{0.3}Fe_2O_4$ as prepared and grinded at 0, 10, 20, 30 and 40 min. The most interesting part of infrared spectra, with respect to Ni–Zn ferrites is 800–400 cm^{-1} range [16]. In this range, ferrites give rise to two most prominent absorption bands

between 800 and 400 cm^{-1}, the ν_1 band is assigned to Fe^{3+}- O^{2-} and Zn^{2+}-O^{2-} stretching vibrations inside the tetrahedral sites. Another absorption band ν_2 is present. This band is assigned to Fe^{3+}-O^{2-} and Ni^{2+}-O^{2-} stretching vibrations inside the octahedral sites. The higher values of ν_1 compared to ν_2 indicate that the normal mode of vibration of the tetrahedral cluster is higher than that of the octahedral cluster. This is attributed to the shorter bond length of the tetrahedral cluster than that of the octahedral cluster [17,18]. In the present system, the band ν_1 lies in the range of 665–545 cm^{-1} and the lower band ν_2 lies in the range of 445–430 cm^{-1}. These bands are common features for all ferrites [16]. A high frequency shoulder of $\nu_1^{\backslash}$ at 775 cm^{-1} has been observed and its intensity increases with increasing grinding time. According to Waldron [16], the presence of divalent ions on tetrahedral sites could explain the existence of a weak shoulder ($\nu_1^{\backslash}$) near 775 cm^{-1}. From Table 2, the position of ν_1 and ν_2 bands shift toward lower frequency with increasing grinding time. The shifts in the band arises from the change in the bond length due to cation redistribution, that causes variations in the cation–oxygen bond length for the octahedral and tetrahedral groups [19,20]. Furthermore, the bands corresponding to 3400, 2920, 1600 and 1050 cm^{-1} represent the stretching and bending vibrations of H–O–H and indicate the presence of free or absorbed water [18,21].

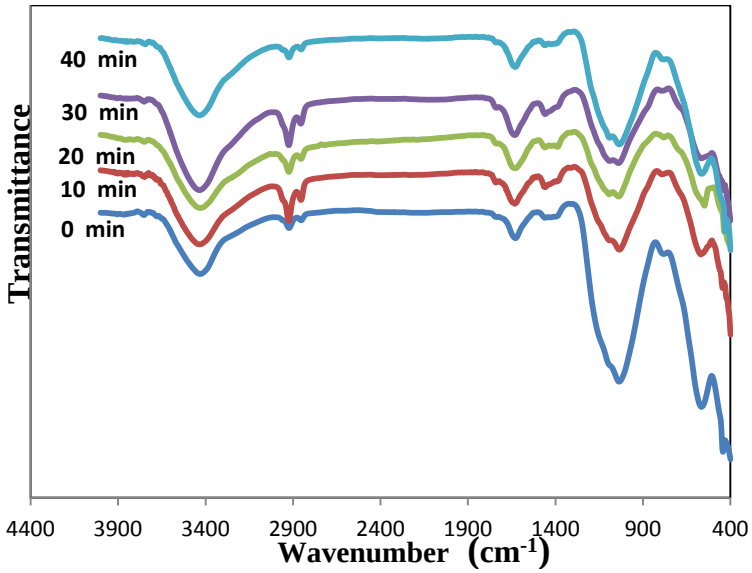

Fig. (3) Infrared spectra of $Ni_{0.7}Zn_{0.3}Fe_2O_4$ grinded at different times.

3.4 Magnetic properties

The magnetic hysteresis loops for $Ni_{0.7}Zn_{0.3}Fe_2O_4$ as prepared and grinded at different times are given in Fig 4. It is clear that, the hysteresis loop areas are very narrow with low values of coercivity (Hc) and remnant magnetization (M_r) which suggest superparamagnetic-like behavior of the nanoparticles. Generally superparamagnetism occurs when the ferromagnetic or ferrimagnetic material is composed of very small crystallites. If the temperature is above the blocking temperature, thermal energy is sufficient to change the direction of magnetization of the entire crystallite. Thus, the hysteresis loops display a remnant magnetization and the coercivity is very small close to zero. This phenomenon is often observed when the magnetic particle size decreases to nano-structure and the magnetic anisotropy energy that keeps the magnetic moment along certain directions is comparable to the thermal fluctuation energy. It can be seen from Fig. 5 that the saturation magnetization value decreases with the decreasing crystallite sizes. [22]. The lower value of saturation magnetization of nanocrystalline ferrites is attributed to surface effects that are due to finite-size scaling of nanocrystallites, which in turn leads to a noncollinearity of

magnetic moments on their surface [23,24]. This can be explained in terms of the core–shell of the nanoparticles consisting of ferrimagnetic aligned core spins and a spin glass-like surface layer. The spin disorder from the surface of the nanoparticles may essentially modify the magnetic properties of these materials, especially when the surface/volume ratio is large [25]. Magnetic properties of ferrites are also a strongly dependent on the cation distribution between tetrahedral (A) and octahedral (B) sites. In mixed Ni–Zn nanoferrites, it has also been reported that some Zn^{2+} ions which normally have strong preference to occupy tetrahedral (A) sites may go into octahedral [B] sites and similarly some Ni^{2+} ion which should go into octahedral [B] sites may also occupy tetrahedral (A) sites [26-28]. Fig. 5 shows the relation between the coercivity (H_c) and grinding time. The coercivity increases with increasing grinding time up to t=30 min and then decreases. This means that the coercivity increases with decreasing crystallite size up to critical size and then decrease. The increase in H_C with decreasing crystallite size happened in multi domain to reach max value of the transition from multi domain to single domain, where the crystallite size decreases below a critical diameter Ds. The coercivity is supposed to vary in the single domain case, according to the relation [29].

$$H_{ci} = g - h/D^{3/2}$$

In multidomain case when the particle diameter is above Ds the coercivity changes as [30]

$$H_{ci} = a + b/D$$

Where D is particle diameter and g, h, a, b are constants.

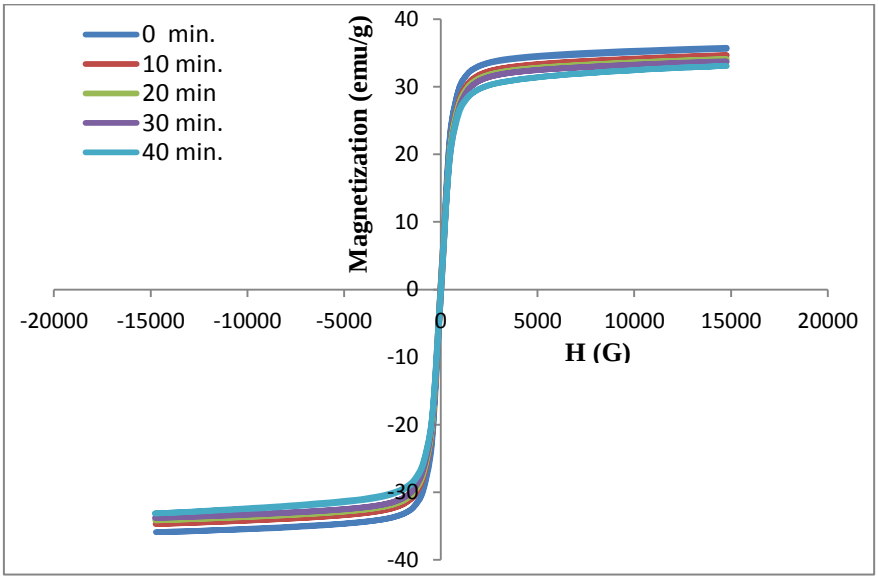

Fig. 4. Hysteresis loops of $Ni_{0.7}Zn_{0.3}Fe_2O_4$ grinded at different times.

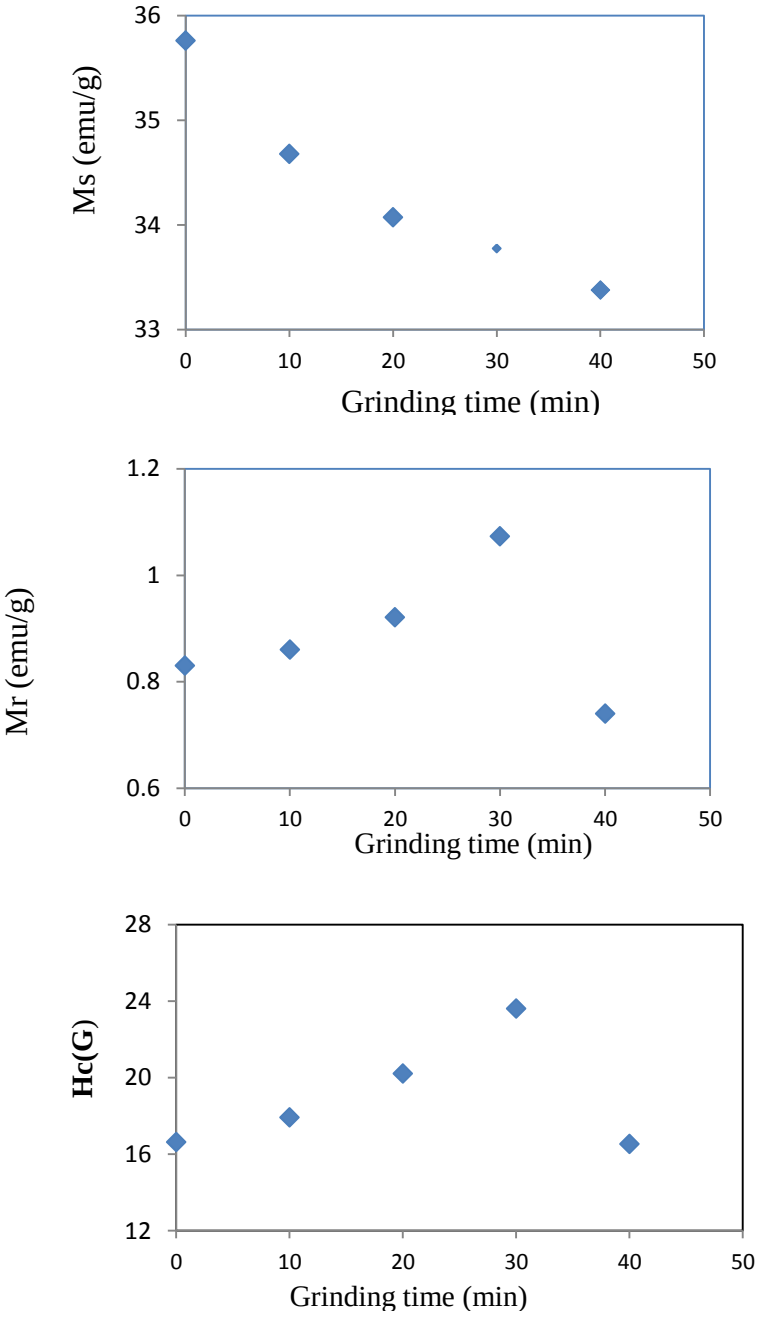

Fig. 5 Saturation magnetization (M_s), remnant magnetization (M_r) and coercive field (H_c) of $Ni_{0.7}Zn_{0.3}Fe_2O_4$ grinded at different times.

4. Conclusion

X-ray diffraction analysis revealed the formation of $Ni_{0.7}Zn_{0.3}Fe_2O_4$ single phase cubic spinel structure of the nanoferrites. The crystallite size calculations showed that they decreased with grinding time. TEM observations revealed that the powders consisted of nanoparticles nearly spherical in shape and agglomerated. The IR spectra show two main absorption bands υ1 (≈575 cm^{-1}) and υ2 (≈ 430 cm^{-1}) and a shoulder near 750 cm^{-1}. Room temperature hysteresis loops reveal superparamagnetic like behavior of the nanoparticles. The saturation magnetization (M_s) is found to be decreasing with grinding time, while the coercivity (Hc) increased with grinding time to a maximum value and then decreased due to transition from multi domain to

single domain state. The properties are suggested that it suitable in target drug delivery application.

References

[1] Y. Shi, J. Ding, X. Liu, J. Wang, J. Magn. Magn. Mater. **205**, 249 (1999).
[2] D.T.T. Nguyet, N.P. Duong, L.T. Hung, T.D. Hien, T. Satoh, J. Alloys Compd. **509**, 6621 (2011).
[3] H.M.I. Abdallah, T. Moyo, J.Z Msomi, J. Phys.: Conf. Ser. **217**, 012141 (2010).
[4] M.A. Gabal, Y.M. AlAngari, Mater. Chem. Phys. **118**, 153 (2009).
[5] D.R. Sharma, RashiMathur, S.R. Vadera, N. Kumar, T.R.N. Kutty, J. Alloys Compd. **358**, 193 (2003).
[6] R.C. Kambale, N.R. Adhate, B.K. Chougle, Y.D. Kolekar, J. Alloys Compd. **49**, 372 (2010).
[7] R.A. Waldron, Ferrites: An Introduction for Microwave Engineers, D. Van Nostrand Company Ltd., London, 1961.
[8] P.S. Anil Kumar, J.J. Shrotri, S.D. Kulkarni, C.E. Deshpande, S.K. Date, Mater. Lett. **27**, 293 (1996).
[9] C.Y. Tsay, K.S. Liu, T.F. Lin, I.N. Lin, J. Magn. Mater. **209**, 189 (2000).
[10] B.V. Bhise, M.B. Dongare, S.A. Patil, S.R. Sawant,J. Mater. Sci. Lett. **10**, 922 (1991).
[11] P.I. Slick, in: E.P. Wohlfarth (Ed.), Ferromagnetic Materials, Vol. 2, North-Holland, Amsterdam, 1980, p. 196.
[12] T. Abraham, Am. Ceram. Soc. Bull. **73,** 62 (1994).
[13] G. Mendoza-SuaHrez et al, J. Magn. Magn.Mater. 223, 55 (2001)
[14] S.D. Shenoy, P.A. Joy, M.R. Anantharaman, J. Magn. Magn. Mater. **269,** 217 (2004).
15- Ponce A.S et al, J. Magn. Magn.Mater., **344**, 182 (2013).
[16] R.D. Waldron, Phys. Rev., **99**(6) , 1727 (1955).
[17] S.A. Mazen, S.F. Mansour, E. Dhahri, H.M. Zaki, T.A. Elmosalami, J. Alloys.Compd. **470**, 294 (2009).
[18] S. Thankachan, B.P. Jacob, S. Xavier, E.M. Mohammed, J. Magn. Magn.Mater. **348,** 140 (2013).
[19] C.B. Kolekar, P.N. Kamble, A.S. Vaingankar, Bull. Mater. Sci. **18**, 133 (1995).
[20] G. Chandrasekaran, S. Selvanandan, K. ManivanNane, J. Mater. Sci. - Mater. Electron. **15**, 15 (2004).
[21] S.S. Kumbhar et al J. Magn. Magn.Mater. **363**, 114 (2014).
[22] Lijun Zhao, Yuming Cui, Hua Yang, Mater. Lett. **60**, 104 (2006).
[23] R.H. Kodama, A.E. Berkowitz, E.J. McNiff Jr., S. Foner, Phys. Rev. Lett. **77,** 394 (1996).
[24] A.E. Berkowitz, J.A. Lahut, I.S. Jacobs, L.M. Levinson, D.W. Forester, Phys. Rev. Lett. **34**, 594 (1975).
[25] C. Caizer, J. Magn. Magn.Mater. **251**, 304 (2002).
[26] B. Parvateeswara Rao, Chong-Oh Kim, Cheo Gi Kim, I. Dumitru, L. Spinu, O. F. Caltun, IEEE Trans. Magn. **42**, 2858 (2006).
[27] E. Ranjith Kumar, R. Jayaprakash, J. Magn. Magn.Mater. **366**, 33 (2014).
[28] T. Slatineanu, A. RalucaIordan, M.N. Palamaru et al., Mater. Res. Bull. **46,** 1455 (2011)
[29] B.D. Cullity, Intrduction to Magnetic Materials, Addison-Wesley Publishing Company, Reading, Massachusetts, 1972.
[30] Robert C. O'Handley, Modern Magnetic Materials, John Wiley & Sons Inc., New York, 2000.